The neuroprotective effects of α7 nicotinic acetylcholine receptor against mutant copper-zinc superoxide dismutase 1-mediated toxicity

Isao Hozumi (hozumi@gifu-pu.ac.jp)
Gifu Yakka Daigaku
Taisei Ito
Gifu Yakka Daigaku
Masatoshi Inden
Gifu Yakka Daigaku
Tomoyuki Ueda
Gifu Yakka Daigaku
Yuta Asaka
Gifu Yakka Daigaku
Hisaka Kurita
Gifu Yakka Daigaku

Research article

Keywords: amyotrophic lateral sclerosis, autophagy, copper-zinc superoxide dismutase 1, α7 nicotinic acetylcholine receptors, PNU282987, TFEB

Posted Date: July 14th, 2020

DOI: https://doi.org/10.21203/rs.3.rs-38218/v1

Abstract

Background

Amyotrophic lateral sclerosis (ALS) is a fatal neurodegenerative disease characterized by the selective and progressive loss of motor neurons. Although many drugs have entered clinical trials, few have shown effectiveness in the treatment of ALS. Previous studies searching for causal genes associated with familial ALS identified the copper-zinc superoxide dismutase 1 (SOD1). Other studies have shown that the stimulation of α7 nicotinic acetylcholine receptor (nAChR) can have neuroprotective effects in some models of neurodegenerative disease, as well as prevent glutamate-induced motor neuronal death. However, the effect of α7 nAChR agonists on mutant SOD1 aggregates in motor neurons remains unclear.

Methods

We examined whether α7 nAChR activation had a neuroprotective effect against $SOD1^{G85R}$-induced toxicity in a cellular model for ALS. Furthermore, the mechanism was also examined by Western blot analysis and qRT-PCR.

Results

We found that α7 nAChR activation showed significant neuroprotective effects against $SOD1^{G85R}$-induced toxicity via the reduction of intracellular protein aggregates. This reduction also correlated with the activation of autophagy through the AMP-activated protein kinase (AMPK)–mammalian target of rapamycin (mTOR) signaling pathway. Furthermore, the activation of α7 nAChRs was found to increase the biogenesis of lysosomes by inducing translocation of the transcription factor EB (TFEB) into the nucleus.

Conclusions

These results support the therapeutic potential of α7 nAChR activation in diseases that are characterized by $SOD1^{G85R}$ aggregates, such as ALS.

Background

Amyotrophic lateral sclerosis (ALS) is an adult-onset neurological disorder that is characterized by muscle weakness and atrophy, paralysis, and eventual death by respiratory failure. Symptoms result from the selective degeneration of upper and lower motor neurons. While 90–95% of ALS cases arise sporadically, 5–10% are familial in Japan. In previous studies searching for causal genes associated with familial ALS, copper-zinc superoxide dismutase 1 (*SOD1*), TAR DNA binding protein of 43 kDa (*TDP43*), fused in sarcoma (*FUS*), and optineurin (*OPTN*) have been identified as playing roles in pathological cascades and phase transitions in sporadic ALS [1–7]. Among familial ALS patients, mutation in SOD1 is a major autosomal dominant inherited allele associated with disease [8].

Several clinical studies suggest a role for glutamate-induced excitotoxicity in familial ALS pathology, although the potential pathogenesis in sporadic ALS is still unclear [9–11]. Previous experiments have shown that rat spinal cord cultures exposed to long-term low-dose glutamate show selective motor neuronal death [12–14]. For this reason, riluzole, a glutamate release inhibitor, has been developed as a therapeutic agent for ALS patients, and has been shown to prolong patient life by several months [15]. Although many drugs have entered into clinical trials, few have demonstrated any effectiveness in the treatment of ALS. Therefore, novel drugs from a new prospective are strongly desired in the clinical field.

Nine α (α2 – α10) and three β (β2 – β4) nicotinic acetylcholine receptor (nAChR) subunits are expressed in the vertebrate brain [16]. These subunits coassemble to form a family of functionally diverse nAChRs. Among nAChR subunits, the most abundant subtypes in the mammalian nervous system are homomeric α7 nAChRs and heteromeric β2 nAChRs, including α4β2 nAChRs [16–19]. These receptors are also widely expressed in the dorsal and ventral horns in the spinal cord [14, 20–22]. Loss of nAChRs is associated with a number of disease states, including Alzheimer's disease, Parkinson's disease (PD), Lewy body disease, schizophrenia, autism, and attention deficit/hyperactivity disorder (ADHD) [23]. In addition, accumulating evidence suggests that α7 nAChRs are important targets in the development of therapeutics for PD. We have previously demonstrated that α7 nAChR activation protects against dopaminergic neuronal death in both acute and chronic animal models of PD induced by 6-hydroxydopamine (6-OHDA) and rotenone, respectively [24, 25].

Nagano et al. have also reported an early decrease in cholinergic input in motor neurons in the spinal cords of patients with ALS [26]. nAChRs have been implicated in neuroprotection mechanisms against acute cell stress induced by excitotoxicity, namely overactivation of glutamate receptors [27]. The stimulation of α7 nAChRs by nicotine actually prevented glutamate-induced motor neuronal death [14]. Therefore, α7 nAChRs represent an important therapeutic target for ALS as well as for PD. Recently, a candidate ALS drug ropinirole (a dopamine D_2 and D_3 receptor agonist used as an antiparkinsonian drug) has been discovered in drug screenings using ALS patient-derived iPS cells, and is now being evaluated in clinical trials for effectiveness [28]. Although the mechanistic details are still unknown, there may be commonalities in the pathological mechanisms of PD and ALS. However, the effect of α7 nAChR agonists against mutant SOD1 aggregates in neurons remains unclear. A pathological hallmark of ALS is the presence of cytoplasmic inclusions or protein aggregates in affected motor neurons, suggesting that impairment of protein degradation may play a role in the disease pathology [29]. SOD1 aggregates are present in both sporadic and familial ALS [30, 31]. In addition, we found that most wild-type SOD1 proteins assume misfolded conformations in cerebrospinal fluid of ALS patients regardless of *SOD1* mutation status [32]. Thus, removal of SOD1 aggregates may be a potential therapeutic approach for ALS treatment. Currently, more than 180 types of SOD1 pathogenic mutations have been identified in ALS patients [33]. Among those, the pathogenic $SOD1^{G85R}$ mutation has been most frequently studied [34, 35, 36, 37].

In the present study, we examined whether α7 nAChR activation exhibited neuroprotective effects against $SOD1^{G85R}$-induced neurotoxicity in a cellular model of ALS.

Material And Methods

Plasmid, cell culture, and transfection

Expression plasmids (pmCherry-N1, Clontech Laboratories Inc., CA, USA) harboring human SOD1 (Wild-type ($SOD1^{WT}$) or mutant ($SOD1^{G85R}$)) were prepared as previously reported [36, 37]. Briefly, N2a cells were maintained in Dulbecco's modified Eagle medium (DMEM, Wako Pure Chemical Industries, Ltd.) containing 10% (v/v) fetal bovine serum (FBS; Thermo Fisher Inc.) under a humidified atmosphere of 5% CO_2 at 37 °C. The cells were passaged by trypsinization every 3–4 days. The transient plasmid expression in N2a cells was accomplished with Lipofectamine 2000 according to the manufacturer's protocol (Thermo Fisher Scientific Inc.).

Thiazolyl Blue Tetrazolium Bromide (MTT) Assay

N2a cells were seeded at 2.0×10^5 cells/ml in 96-well plates in DMEM containing 10% FBS. Following plasmid transfection, the cells were differentiated for 48 h in low glucose (1.0 g/l) DMEM supplemented with 2% FBS and 2 mM N,N-dibutyladenosine 3',5'-phosphoric acid (dbcAMP; Nacalai Tesque Inc.) with 0.1 or 1 μM PNU282987 (Wako Pure Chemical Industries Ltd.) in the presence or absence of 20 μM methyllycaconitine (MC; Cayman Chemical Ltd.) or 20 μM chloroquine (CQ; Tokyo Chemical Industry Ltd.) for 24 h. The number of live cells was estimated by Cell Counting Kit-8, following the manufacturer's instructions (Wako Pure Chemical Industries Ltd.). Briefly, the reagent was added into the wells and the plate was incubated at 37 °C for 3 h. Cell viability was calculated through the detection of the optical density of formazan at 450 nm using GloMax® (Promega). A 600 nm wavelength was used as reference.

Aggregation rate analysis

We performed aggregation assay based on previous studies [36, 37]. Briefly, after 24 h of mCherry-fused $SOD1^{WT}$ or $SOD1^{G85R}$ vector transfection, the cells were treated with PNU282987 in the presence or absence of 20 μM MC or 20 μM CQ for 24 h. Subsequently, the cells were washed twice with PBS for 5 min and fixed with 4% paraformaldehyde for 15 min. Fluorescent microscopy images were acquired with a confocal fluorescence microscope (LSM700, Carl Zeiss). For counting the number of aggregates, we used IN Cell Investigator 2200 (GE Healthcare). In each experiment, at least 3000 cells were counted.

Immunoblotting

After treatment, the cells were lysed with TNE lysis buffer (50 mM Tris-HCl (pH. 7.4), 150 mM NaCl, 1 mM ethylenediamineteraacetic acid, protease inhibitor cocktail) containing 1% Triton X and then were centrifuged at 15,000 × g at 4 °C for 5 min. The supernatant protein sample was collected. Protein concentrations were quantified using a BCA protein assay kit (Thermo Fisher Scientific Inc.) with bovine serum albumin (BSA) as a standard. Lysates were mixed with sample buffer containing 10% 2-mercaptoethanol, and subjected to 10% SDS-polyacrylamide gel electrophoresis (SDS-PAGE). SDS-PAGE was performed under constant voltage of 200V at room temperature for 40 min. The separated proteins in polyacrylamide gel were transferred to a PVDF membrane in transfer buffer (0.3% Tris, 1.44% glycine,

20% methanol) under constant voltage of 100V at 4 °C for 90 min. The membranes were incubated with 5% BSA (Wako) for 60 min, and then with following primary antibodies for overnight: mouse monoclonal antibody against β-actin (1: 2000, Santa Cruz Biotechnology) and rabbit polyoclonal antibodies against LC-3 (1:1000, Cell Signaling), p-AMPK (1:1000, Cell Signaling Technology), p-mTOR (1:1000, Cell Signaling Technology), mTOR(1:1000, Cell Signaling Technology), p62 (1:1000, Cell Signaling Technology), TFEB (1:1000, Proteintech). After the primary antibody reaction, the membrane was incubated in the secondary antibody (goat anti-rabbit antibody conjugated with HRP (1:2500, Santa Cruz Biotechnology) or goat anti-mouse HRP antibody conjugated with HRP (1:2500, Santa Cruz Biotechnology)). The membrane was incubated in ECL prime (GE Healthcare, Buckinghamshire, UK) to generate the chemiluminescence from HRP antibodies. The chemiluminescence was detected by Fusion System (Vilber-Lourmat). The band density was measured using ImageJ.

RNA preparation and qRT-PCR

Reverse transcription was performed using the ReverTra Ace qPCR RT Master Mix, in accordance with the manufacturer's instructions (TOYOBO). qRT-PCR was performed using SYBR Green on a StepOne Real-Time PCR System, in accordance with the manufacturer's instructions (Life Technologies). The sequences of gene-specific primer sets are shown in **Table 1**. The expression levels of mRNA were normalized to the expression levels of β-actin mRNA.

Immunostaining

At 24 h after transfection of each vector into N2a cells, the cells were treated with 1 μM PNU298987 in the presence or absence 1 μM STO609 or 1 μM 1,2-bis (2-aminophenoxy) ethane-N,N,N0,N0-tetraacetic acid tetrakis (acetoxymethyl ester) (BAPTA-AM). At 24 h after the treatment, cells were fixed by 4% paraformaldehyde and then permeabilized with 0.1% Triton X-100 diluted in PBS. To block the reaction, the cells were treated with 2% goat serum for 60 min. The cells were incubated with rabbit polyclonal antibody against TFEB (1:200, Proteintech) at 4 °C for overnight. Subsequently, the cells were incubated with secondary antibody (goat anti-rabbit antibody Alexa 488) at room temperature for 1 h. In addition, nuclear staining was performed with Hoechst 33342 (Molecular Probes). Fluorescent microscopy images were acquired with a confocal fluorescence microscope (LSM700, Carl Zeiss).

Lysosomal staining

N2a cells were seeded at 1.0×10^5 cells/ml in CELLview™ cell culture dishes (Greiner Bio-one). At 24 h after transfection to N2a cells each vector, the cells were treated with 1 μM PNU298987 in the presence or absence 1 μM STO609 or 1 μM BAPTA-AM. At 24 h after the treatment, lysosomes were stained with LysoTracker™ Green DND-26 (Thermo Fisher Scientific) and nucelei were stained with Hoechst 33342 (Thermo Fisher Scientific), in accordance with the manufacturer's instructions (Thermo Fisher Scientific). Fluorescent microscopy images were acquired with a confocal fluorescence microscope (LSM700, Carl Zeiss). Image analysis was performed using ImageJ.

Cell fractions preparation

At 24 h after transfection of each vector into N2a cells, the cells were treated with 1 μM PNU298987 in the presence or absence 1 μM STO609 or 1 μM BAPTA-AM. At 24 h after the treatment, 1.0×10^6 cells were harvested with trypsin-EDTA and nuclear extraction was performed using NE-PER™ Nuclear and Cytoplasmic Extraction Reagents, in accordance with the manufacturer's instructions (Thermo Fisher Scientific). To assess the purity of the fractionation, the cytoplasmic and nuclear fractions were confirmed by immunoblotting using anti-GAPDH (1:1000, MBL Ltd.) as a cytoplasmic marker and anti-Histone H3 (1:1000, Cell Signaling Technology Ltd.) as a nuclear marker.

Statistical analysis

Data are given as the mean ± standard error of the mean (SEM). Significance was determined using the Student's t test or analysis of variance. Further statistical analysis for post hoc comparisons was performed using the Bonferroni/Dunn test (StatView, Abacus). p-values of less than 0.05 were considered to be statistically significant.

Results

The α7 nAChR agonist reduces intracellular $SOD1^{G85R}$ aggregates and prevents neurotoxicity of $SOD1^{G85R}$

Previously, aggregate formation was confirmed in mCherry-fused $SOD1^{G85R}$ (hereafter $SOD1^{G85R}$)-transfected N2a cells, which contributed to cell death via the formation of triton X-100-insoluble aggregates [36–39]. To investigate the effect of α7 nAChR activation on $SOD1^{G85R}$ aggregate formation, we evaluated the number of intracellular aggregates with an Imaging Cytometer after treatment with PNU282987, an α7 nAChR selective agonist (Fig. 1). $SOD1^{G85R}$ formed intracellular aggregates in approximately 25% of transfected N2a cells. PNU282987 treatment significantly reduced the percentage of cells with intracellular $SOD1^{G85R}$ aggregates (Fig. 1A,B). This reduction in aggregate formation was markedly blocked by methyllycaconitine (MC), an α7 nAChR antagonist (Fig. 1A, B). In order to examine the effect of PNU282987 on $SOD1^{G85R}$-mediated neurotoxicity, we performed a MTT assay in differentiated N2a cells (Fig. 1C). Although transfection of $SOD1^{WT}$ did not affect cell survival, transfection of $SOD1^{G85R}$ severely induced cell death. PNU282987 prevented $SOD1^{G85R}$-induced cell death; in addition, methyllycaconitine significantly inhibited the PNU282987-induced neuroprotection (Fig. 1C). These results suggest that α7 nAChR activation exerts significant neuroprotective effects against $SOD1^{G85R}$-induced toxicity via the reduction of intracellular protein aggregates.

The α7 nAChR agonist exerts neuroprotective effects against $SOD1^{G85R}$ aggregation via activation of autophagy

To analyze the mechanism of the reduction of intracellular aggregates upon α7 nAChR activation, we focused on autophagy, a prominent protein degradation pathway. Western blot analysis showed that PNU282987 treatment increased the formation of LC3-II, a marker of autophagy, in N2a cells (Fig. 2A). PNU282987 treatment also significantly decreased p62 protein levels, a marker of selective autophagy (Fig. 2B). In addition, chloroquine (CQ), an inhibitor of autophagy, prevented the reduction of cytoplasmic

aggregation of $SOD1^{G85R}$ induced by PNU282987 (Fig. 2C, D). To further investigate whether the neuroprotective effects of PNU282987 were associated with autophagy, we performed a MTT assay in the presence of chloroquine. The protective effect of PNU282987 was significantly inhibited by chloroquine treatment (Fig. 2E). These data suggest that PNU282987 treatment reduces the quantity of subcellular aggregates via the upregulation of autophagy, which prevented $SOD1^{G85R}$-associated neurotoxicity.

α7 nAChR activation promotes autophagy via Ca^{2+} influx and the AMP-activated protein kinase (AMPK)-mammalian target of rapamycin (mTOR) signaling pathway

α7 nAChR activation increases intracellular Ca^{2+} influx through the α7 receptor channel. It is well-established that Ca^{2+} influx is a regulator of autophagy [40]. To elucidate the pathways involved in elevated Ca^{2+} influx after α7 nAChR activation, we used the cell-permeable cytosolic Ca^{2+} chelator BAPTA-AM. Pre-treatment with BAPTA-AM significantly inhibited the formation of LC3-II and the reduction in p62 protein induced by PNU282987 (Fig. 3A-C). CaMKKβ has been proposed as a potential target of cytosolic Ca^{2+} signaling [41], although direct evidence remains elusive. Similar to the effects of BAPTA-AM, the formation of LC3-II and the reduction in p62 induced by PNU282987 were significantly inhbited by STO609, a CaMKKβ-specific inhibitor (Figs. 3A-C).

The AMP-activated protein kinase (AMPK)–mammalian target of rapamycin (mTOR) signaling pathway is downstream of Ca^{2+} signaling and plays an important role in the regulation of autophagy in response to different stress conditions [42]. To further identify the signal transduction pathway mediated by PNU282987, we investigated the AMPK–mTOR pathway. PNU282987 significantly increased AMPK phosphorylation and significantly inhibited mTOR phosphorylation (Figs. 3A, D-E). In addition, BAPTA-AM and STO609 pre-treatment significantly decreased PNU282987-dependent AMPK phosphorylation and restored mTOR phosphorylation (Fig. 3A, D-E), suggesting activation of the AMPK pathway and inhibition of the mTOR pathway occurs via Ca^{2+} influx following α7 nAChR activation. These results suggest that α7 nAChR activation potentially induces autophagy via Ca^{2+} influx and signaling through the AMPK and mTOR pathways.

α7 nAChR agonist promotes lysosomal biogenesis via nuclear translocation of transcription factor EB (TFEB)

AMPK signaling activates transcription factor EB (TFEB), which is a potential key transcription in the induction of autophagy upon its dephosphorylation and nuclear translocation [43]. TFEB can enter the nucleus and bind to the E-box of the CLEAR element, which regulates the transcription of genes associated with the biogenesis of lysosomes and autophagosomes [44]. We first analyzed mRNA levels of lysosomes and autophagy-related genes whose transcription could be regulated by TFEB using qRT-PCR. The mRNA levels of lysosomal-related genes (such as *Lamp1*, *Lamp2*, *Npc1*, and *Tpp1*) and autophagy-related genes (such as *Becn1, Map1lc3b, Sqstm1*, and *Uvrag*) were significantly up-regulated in response to PNU282987 treatment (Fig. 4). Upregulation of these mRNAs was markedly blocked by pre-treatment with BAPTA-AM and STO609 (Fig. 4).

Next, we examined the distribution of TFEB in the $SOD1^{G85R}$-transfected N2a cells after PNU282987 treatment using immunofluorescence (Fig. 5A). TFEB levels in the nucleus were increased following PNU282987 treatment. Meanwhile, TFEB levels in the cytoplasm were decreased by PNU282987 (Fig. 5A). Western blot also demonstrated that PNU282987 treatment decreased and increased TFEB levels in cytoplasmic and nuclear fractions, respectively (Fig. 5B, C). In addition, nuclear translocation of TFEB induced by PNU282987 was significantly inhibited following pre-treatment with BAPTA-AM and STO609 (Fig. 5B, C). We next determined whether PNU282987 enhances lysosomal biogenesis using immunofluorescence (Fig. 5D, E). PNU282987 promoted lysosomal biogenesis as quantified by fluorescence intensity in LysoTracker-stained cells. The effect of PNU282987 on lysosomal biogenesis was inhibited by pre-treatment with BAPTA-AM and STO609 (Fig. 5D, E). Together, these data suggest that α7 nAChRs activation promotes lysosomal biogenesis via the nuclear transposition of TFEB.

Discussion

The goal of the present study was to determine whether activation of α7 nAChR had a neuroprotective effect against $SOD1^{G85R}$ aggregate-induced toxicity in a cellular model of ALS. We demonstrated that PNU282987, an α7 nAChR selective agonist, induces significant neuroprotective effects via reduction of $SOD1^{G85R}$ intracellular aggregates. This reduction strongly correlated with the activation of autophagy via the AMPK–mTOR signaling pathway. Furthermore, PNU282987 increased lysosome biogenesis by promoting TFEB translocation into the nucleus. These findings identify α7 nAChR as a novel neuroprotective target against the $SOD1^{G85R}$ aggregate-mediated neurotoxicity.

Autophagy dysfunction has been implicated in various neurodegenerative diseases, including ALS [45, 46]. The notion that autophagy dysfunction contributes to ALS pathogenesis is strongly supported by the identification of numerous genes associated with familial ALS also involved in regulation of autophagy, including *SQSTM1* [47], *OPTN* [4], *TBK1* [48], and *VCP* [49]. The presence of intracellular, insoluble inclusions composed of misfolded proteins is a hallmark of ALS pathology [29]. Therefore, removal of SOD1 aggregates may represent one potential therapeutic approach for ALS treatment.

There are two major pathways for cellular protein degradation: the ubiquitin proteasome system (UPS), and autophagy. Autophagy has been shown to degrade both soluble and aggregated protein substrates that are too large to pass through the pore of the proteasome, such as the toxic SOD1 protein aggregates, while UPS primarily degrades soluble SOD1, suggesting that autophagy regulation is critical for improving ALS pathology [46, 50].

Treatment of mutant SOD1 transgenic mice with trehalose resulted in increased life span, improved neuronal survival, reduced astrogliosis, and delayed disease onset via activation of autophagy [51]. Similarly, carbamazepine treatment activated autophagy via the AMPK-ULK1 signaling pathway and promoted the clearance of mutant SOD1 aggregates. Carbamazepine treatment also delayed disease onset and extended life span of $SOD1^{G93A}$ mice [52]. In our previous studies, autophagy induction has demonstrated beneficial effects in cells harboring pathogenic SOD1 mutations [36, 37, 53]. In addition to

pharmacological studies, genetic ablation of XBP-1 (X-box-binding protein) in motor neurons of $SOD1^{G85R}$ mice enhanced the clearance of mutant SOD1 aggregates and increased survival via activation of autophagy [54]. Moreover, bosutinib, which boosts autophagy, can improve the survival of iPSC-derived motor neurons from patients with familial ALS caused by mutations in SOD1 [55].

Conversely, abnormalities (activations) in autophagy have been observed in numerous neurodegenerative diseases, including ALS [56]. Pharmacological and genetic modulation of autophagy may result in diverse and even detrimental outcomes to the survival of ALS models; interventions targeting genes including mSOD1, FUS and TDP-43 [46, 50] have shown that it may be necessary to jointly consider the specific effects of each individual mutation, pathology, and possibly other context-dependent influences. These results suggest the need for developing autophagy inducers with higher specificity and lower cytotoxicity based on ALS pathology [50]. In the present study, PNU282987 exerted neuroprotective effects against $SOD1^{G85R}$-induced toxicity via autophagy activation. Although it is necessary to explore this finding further with iPS cells and animal models, among candidates of autophagy inducers, α7 nAChR may be a promising candidate.

Our study indicates that PNU282987 decreased mTOR phosphorylation and increased AMPK phosphorylation, and subsequently induced autophagy. The AMPK–mTOR signaling pathway is a downstream target of Ca^{2+} signaling and plays an important role in the regulation of autophagy in response to different stresses [42]. In support of this, we showed that AMPK and mTOR phosphorylation were significantly affected by pre-treatment with BAPTA-AM and STO609, indicating activation of the AMPK pathway and inhibition of the mTOR pathway via Ca^{2+} influx following α7 nAChR activation. In addition, AMPK phosphorylation activates TFEB, which is a potential key transcription for autophagy induction upon its dephosphorylation and nuclear translocation [43]. It has been reported that under stress conditions or upon loss of function, TDP43 can regulate the nuclear translocation of TFEB in order to promote the transcription of autophagic genes. This indicates that TFEB may play a role in potential strategies for ALS treatment. In the present study, PNU282987 significantly increased the mRNA levels of *Lamp1*, *Lamp2*, *Npc1*, *Tpp1, Becn1, Map1lc3b, Sqstm1, and Uvrag* the transcription of which could be regulated by TFEB. In addition, PNU282987 significantly increased the TFEB translocation into the nucleus and promoted lysosomal biogenesis. Previously, trehalose, an enhancer of mTOR-independent autophagy, was shown to delay ALS onset and reduce motor neuron loss in $SOD1^{G93A}$ mice [57]. In contrast, mTOR-dependent activation of autophagy resulted in loss of motor neurons and reduced survival in the same ALS mouse model, which may be due to other physiological functions of mTOR inhibition [58]. The neuroprotective effects of α7 nAChR activation may be due to pleiotropic effects, it will be necessary to conduct further studies.

ALS is a multifactorial disease encompassing a network of cellular pathways [59]. Drugs with pleiotropic effects may be practically more effective than drugs with a single effect for patients with ALS. As α7 nAChR activation has various neuroprotective effects including autophagy activation, α7 nAChR activation may possess novel therapeutic potential for ALS.

Conclusion

Stimulation of α7 nAChR showed a neuroprotective effect against $SOD1^{G85R}$ aggregate-induced toxicity in a cellular model of ALS. It was suggested that this effect is due to activation of autophagy by AMPK-mTOR pathway and TFEB translocation into the nucleus. These results support the therapeutic potential of α7 nAChR activation in diseases that are characterized by $SOD1^{G85R}$ aggregates, such as ALS.

Declarations

Acknowledgments & Funding

This work was supported by grants from the Takeda Science Foundation, the Japan Society for the Promotion of Science (JSPS) KAKENHI (Grant No. JP17K08311), Grant-in-Aid for Scientific Research on Innovative Areas JSPS KAKENHI (Grant No. JP19H05767A02), Nagai Memorial Research Scholarship from the Pharmaceutical Society of Japan, the API Research Foundation and Smoking Research Foundation.

Availability of data and materials

The datasets used and/or analysed during the current study are available from the corresponding author on reasonable request.

Author Contributions

T. Ito, M. Inden and I. Hozumi designed and organized the project. T. Ito, T. Ueda, Y. Asaka and H. Kurita performed the experiments. T. Ito, M. Inden and I. Hozumi wrote the paper. All authors read and approved the final manuscript.

Ethics approval and consent to participate

Not applicable.

Consent for publication

Not applicable.

Competing Interests

The authors declare that they have no competing interests.

Author information

Not applicable.

Publisher's Note

Author details

[1]Laboratory of Medical Therapeutics and Molecular Therapeutics, Gifu Pharmaceutical University, Gifu 501-1196, Japan.

References

1. Rosen DR, Siddique T, Patterson D, Figlewicz DA, Sapp P, Hentati A, *et al*. Mutations in Cu/Zn superoxide dismutase gene are associated with familial amyotrophic lateral sclerosis. *Nature.* 1993; **362**: 59-62. doi: 10.1038/362059a0.

2. Neumann M, Sampathu DM, Kwong LK, Truax AC, Micsenyi MC, Chou TT, et al. Ubiquitinated TDP-43 in frontotemporal lobar degeneration and amyotrophic lateral sclerosis. *Science*. 2006; **314**: 130-3. doi: 10.1126/science.1134108.

3. Kwiatkowski TJ Jr, Bosco DA, Leclerc AL, Tamrazian E, Vanderburg CR, Russ C, et al. Mutations in the FUS/TLS gene on chromosome 16 cause familial amyotrophic lateral sclerosis. *Science.* 2009; **323**: 1205-8. doi: 10.1126/science.1166066.

4. Maruyama H, Morino H, Ito H, Izumi Y, Kato H, Watanabe Y, et al. Mutations of optineurin in amyotrophic lateral sclerosis. *Nature.* 2010; **465**: 223-6. doi: 10.1038/nature08971. Epub 2010 Apr 28.

5. Da Cruz S, Cleveland DW. Understanding the role of TDP-43 and FUS/TLS in ALS and beyond. *Curr Opin Neurobiol.* 2011; **21**: 904-19. doi: 10.1016/j.conb.2011.05.029.

6. Taylor JP, Brown RH Jr, Cleveland DW. Decoding ALS: from genes to mechanism. *Nature*. 2016; **539**: 197-206. doi: 10.1038/nature20413.

7. Fujimori K, Ishikawa M, Otomo A, Atsuta N, Nakamura R, Akiyama T, et al. Modeling sporadic ALS in iPSC-derived motor neurons identifies a potential therapeutic agent. *Nat Med*. 2018; **24**: 1579-1589. doi: 10.1038/s41591-018-0140-5. Epub 2018 Aug 20.

8. Julien JP. Amyotrophic lateral sclerosis. unfolding the toxicity of the misfolded. *Cell.* 2001; **104**: 581-91. doi: 10.1016/s0092-8674(01)00244-6.

9. Bensimon G, Lacomblez L, Meininger V. A controlled trial of riluzole in amyotrophic lateral sclerosis. ALS/Riluzole Study Group. *N Engl J Med.* 1994; **330**: 585-91. doi: 10.1056/NEJM199403033300901.

10. Couratier P, Hugon J, Sindou P, Vallat JM, Dumas M. Cell culture evidence for neuronal degeneration in amyotrophic lateral sclerosis being linked to glutamate AMPA/kainate receptors. *Lancet.* 1993; **341**: 265-8. doi: 10.1016/0140-6736(93)92615-z.

11. Rothstein JD, Van Kammen M, Levey AI, Martin LJ, Kuncl RW. Selective loss of glial glutamate transporter GLT-1 in amyotrophic lateral sclerosis. *Ann Neurol*. 1995; **38**: 73-84. doi: 10.1002/ana.410380114.

12. Urushitani M, Shimohama S, Kihara T, Sawada H, Akaike A, Ibi M, et al. Mechanism of selective motor neuronal death after exposure of spinal cord to glutamate: involvement of glutamate-induced nitric oxide in motor neuron toxicity and nonmotor neuron protection. *Ann Neurol.* 1998; **44**: 796-807. doi: 10.1002/ana.410440514.

13. Kanki R, Nakamizo T, Yamashita H, Kihara T, Sawada H, Uemura K, et al. Effects of mitochondrial dysfunction on glutamate receptor-mediated neurotoxicity in cultured rat spinal motor neurons. *Brain Res.* 2004 **1015**, 73-81. doi: 10.1016/j.brainres.2004.04.044.

14. Nakamizo T, Kawamata J, Yamashita H, Kanki R, Kihara T, Sawada H, et al. Stimulation of nicotinic acetylcholine receptors protects motor neurons. *Biochem Biophys Res Commun.* 2005; **330**: 1285-9. doi: 10.1016/j.bbrc.2005.03.115.

15. Lucette L, Bensimon G, Leigh PN, Guillet P, Meininger V. Dose-ranging study of riluzole in amyotrophic lateral sclerosis. Amyotrophic Lateral Sclerosis/Riluzole Study Group II. *Lancet.* 1996; **347**: 1425–31. doi: 10.1016/s0140-6736(96)91680-3.

16. Faure P, Tolu S, Valverde S, Naudé J. Role of nicotinic acetylcholine receptors in regulating dopamine neuron activity. *Neuroscience.* 2014; **282C**: 86-100. doi: 10.1016/j.neuroscience.2014.05.040.

17. Gotti C, Zoli M, Clementi F. Brain nicotinic acetylcholine receptors: native subtypes and their relevance. *Trends Pharmacol Sci.* 2006; **27**: 482-91. doi: 10.1016/j.tips.2006.07.004.

18. Taly A, Corringer PJ, Guedin D, Lestage P, Changeux JP. Nicotinic receptors: allosteric transitions and therapeutic targets in the nervous system. *Nat Rev Drug Discov.* 2009; **8**: 733-50. doi: 10.1038/nrd2927.

19. Rode F, Munro G, Holst D, Nielsen EØ, Troelsen KB, Timmermann DB, et al. Positive allosteric modulation of α4b2 nAChR agonist induced behaviour. *Brain Res.* 2012; **1458**: 67-75. doi: 10.1016/j.brainres.2012.03.064. Epub 2012 Apr 4.

20. Kiyosawa A, Katsurabayashi S, Akaike N, Pang ZP, Akaike N. Nicotine facilitates glycine release in the rat spinal dorsal horn. *J Physiol.* 2001; **536**: 101-10. doi: 10.1111/j.1469-7793.2001.t01-1-00101.x.

21. Roth AL, Berg DK. Large clusters of alpha7-containing nicotinic acetylcholine receptors on chick spinal cord neurons. *J Comp Neurol.* 2003; **465**: 195-204. doi: 10.1002/cne.10856.

22. Takeda D, Nakatsuka T, Gu JG, Yoshida M. The activation of nicotinic acetylcholine receptors enhances the inhibitory synaptic transmission in the deep dorsal horn neurons of the adult rat spinal cord. *Mol Pain.* 2007; **3**: 26. doi: 10.1186/1744-8069-3-26.

23. Shimohama S. Nicotinic receptor-mediated neuroprotection in neurodegenerative disease models. *Biol Pharm Bull*. 2009; **32**: 332-6. doi: 10.1248/bpb.32.332.

24. Yanagida T, Takeuchi H, Kitamura Y, Takata K, Minamino H, Shibaike T, et al. Synergistic effect of galantamine on nicotine-induced neuroprotection in hemiparkinsonian rat model. *Neurosci Res* 2008; **62**: 254-61. doi: 10.1016/j.neures.2008.09.003. Epub 2008 Sep 20.

25. Takeuchi H, Yanagida T, Inden M, Takata K, Kitamura Y, Yamakawa K, et al. Nicotinic receptor stimulation protects nigral dopaminergic neurons in rotenone-induced Parkinson's disease models. *J Neurosci Res.* 2009; **87**: 576-585. doi: 10.1002/jnr.21869.

26. Nagao M, Misawa H, Kato S, Hirai S. Loss of cholinergic synapses on the spinal motor neurons of amyotrophic lateral sclerosis. *J Neuropathol Exp Neurol*. 1998; **57**: 329-33. doi: 10.1097/00005072-199804000-00004.

27. Kaur J, Rauti R, Nistri A. Nicotine-mediated neuroprotection of rat spinal networks against excitotoxicity. *Eur J Neurosci*. 2018; **47**: 1353-1374. doi: 10.1111/ejn.13950. Epub 2018 Jun 3.

28. Okano H, Yasuda D, Fujimori K, Morimoto S, Takahashi S. Ropinirole, a New ALS Drug Candidate Developed Using iPSCs. *Trends Pharmacol Sci*. 2020; **41**: 99-109. doi: 10.1016/j.tips.2019.12.002. Epub 2020 Jan 8.

29. Blokhuis AM, Groen EJ, Koppers M, van den Berg LH, Pasterkamp RJ. Protein aggregation in amyotrophic lateral sclerosis. *Acta Neuropathol*. 2013; **125**: 777–94. doi: 10.1007/s00401-013-1125-6.

30. Bosco DA, Morfini G, Karabacak NM, Song Y, Gros-Louis F, Pasinelli P, et al. Wild-type and mutant SOD1 share an aberrant conformation and a common pathogenic pathway in ALS. *Nat Neurosci.* 2010; **13**: 1396-1403. doi: 10.1038/nn.2660. Epub 2010 Oct 17.

31. Forsberg K, Jonsson PA, Andersen PM, Bergemalm D, Graffmo KS, Hultdin M, et al. Novel antibodies reveal inclusions containing non-native SOD1 in sporadic ALS patients. *PLoS One.* 2010; **5**: e11552. doi: 10.1371/journal.pone.0011552.

32. Tokuda E, Takei YI, Ohara S, Fujiwara N, Hozumi I, Furukawa Y. Wild-type Cu/Zn-superoxide dismutase is misfolded in cerebrospinal fluid of sporadic amyotrophic lateral sclerosis. *Mol Neurodegener*. 2019; **14**: 42. doi: 10.1186/s13024-019-0341-5.

33. Huai J, Zhang Z. Structural Properties and Interaction Partners of Familial ALS-Associated SOD1 Mutants. *Front Neurol*. 2019; **10**: 527. doi: 10.3389/fneur.2019.00527. eCollection 2019.

34. Abel O, Powell JF, Andersen PM, Al-Chalabi A. ALSoD: A user-friendly online bioinformatics tool for amyotrophic lateral sclerosis genetics. *Hum Mutat*. 2012; **33**: 1345-51. doi: 10.1002/humu.22157. Epub 2012 Jul 16.

35. Peters OM, Ghasemi M Jr, Brown RH. Emerging mechanisms of molecular pathology in ALS. *J Clin Invest*. 2015; **125**: 2548. doi: 10.1172/JCI82693. Epub 2015 Jun 1.

36. Ueda T, Inden M, Shirai K, Sekine SI, Masaki Y, Kurita H, et al. The effects of Brazilian green propolis that contains flavonols against mutant copper-zinc superoxide dismutase-mediated toxicity. *Sci Rep.* 2017; **7**: 2882. doi: 10.1038/s41598-017-03115-y.

37. Ueda T, Inden M, Asaka Y, Masaki Y, Kurita H, Tanaka W, et al. Effects of gem-dihydroperoxides against mutant copper-zinc superoxide dismutase-mediated neurotoxicity. *Mol Cell Neurosci*. 2018; **92**: 177-184. doi: 10.1016/j.mcn.2018.09.001. Epub 2018 Sep 5.

38. Oh YK, Shin KS, Yuan J, Kang SJ. Superoxide dismutase 1 mutants related to amyotrophic lateral sclerosis induce endoplasmic stress in neuro2a cells. *J Neurochem*. 2008; **104**: 993-1005. doi: 10.1111/j.1471-4159.2007.05053.x.

39. Watanabe S, Hayakawa T, Wakasugi K, Yamanaka K. Cystatin C protects neuronal cells against mutant copper-zinc superoxide dismutase-mediated toxicity. *Cell Death Dis.* 2014; **5**: e1497. doi: 10.1038/cddis.2014.459.

40. Jing Z, Sui X, Yao J, Xie J, Jiang L, Zhou Y, et al. SKF-96365 activates cytoprotective autophagy to delay apoptosis in colorectal cancer cells through inhibition of the calcium/CaMKIIγ/AKT-mediated pathway. *Cancer Lett.* 2016; **372**: 226-38. doi: 10.1016/j.canlet.2016.01.006. Epub 2016 Jan 20.

41. Scotto Rosato A, Montefusco S, Soldati C, Di Paola S, Capuozzo A, Monfregola J, et al. TRPML1 links lysosomal calcium to autophagosome biogenesis through the activation of the CaMKKβ/VPS34 pathway. *Nat Commun.* 2019; **10**: 5630. doi: 10.1038/s41467-019-13572-w.

42. Jin Y, Bai Y, Ni H, Qiang L, Ye L, Shan Y, et al. Activation of autophagy through calcium-dependent AMPK/mTOR and PKCθ pathway causes activation of rat hepatic stellate cells under hypoxic stress. *FEBS Lett.* 2016; **590**: 672-82. doi: 10.1002/1873-3468.12090. Epub 2016 Mar 1.

43. Collodet C, Foretz M, Deak M, Bultot L, Metairon S, Viollet B, et al. AMPK promotes induction of the tumor suppressor FLCN through activation of TFEB independently of mTOR. *FASEB J.* 2019; **33**: 12374-91. doi: 10.1096/fj.201900841R. Epub 2019 Aug 19.

44. Wu H, Chen H, Zheng Z, Li J, Ding J, Huang Z, et al. Trehalose promotes the survival of random-pattern skin flaps by TFEB mediated autophagy enhancement. *Cell Death Dis.* 2019; **10**: 483. doi: 10.1038/s41419-019-1704-0.

45. Beltran S, Nassif M, Vicencio E, Arcos J, Labrador L, Cortes BI, et al. Network approach identifies Pacer as an autophagy protein involved in ALS pathogenesis. *Mol Neurodegener.* 2019; **14**: 14. doi: 10.1186/s13024-019-0313-9.

46. Djajadikerta A, Keshri S, Pavel M, Prestil R, Ryan L, Rubinsztein DC. Autophagy induction as a therapeutic strategy for neurodegenerative diseases. *J Mol Biol.* 2020; **432**: 2799-2821. doi: 10.1016/j.jmb.2019.12.035. Epub 2019 Dec 27.

47. Fecto F, Yan J, Vemula SP, Liu E, Yang Y, Chen W, et al. sSQSTM1 mutations in familial and sporadic amyotrophic lateral sclerosis. *Arch Neurol.* 2011; **68**: 1440-6. doi: 10.1001/archneurol.2011.250.

48. Cirulli ET, Lasseigne BN, Petrovski S, Sapp PC, Dion PA, Leblond CS, et al. Exome sequencing in amyotrophic lateral sclerosis identifies risk genes and pathways. *Science.* 2015; **347**: 1436-41. doi: 10.1126/science.aaa3650. Epub 2015 Feb 19.

49. Johnson JO, Mandrioli J, Benatar M, Abramzon Y, Van Deerlin VM, Trojanowski JQ, et al. Exome sequencing reveals VCP mutations as a cause of familial ALS. *Neuron.* 2010; **68**: 857-64. doi: 10.1016/j.neuron.2010.11.036.

50. Zhang X, Chen S, Lu K, Wang F, Deng J, Xu Z, et al. Verapamil Ameliorates Motor Neuron Degeneration and Improves Lifespan in the SOD1^{G93A} Mouse Model of ALS by Enhancing Autophagic Flux. *Aging Dis.* 2019; **10**: 1159-73. doi: 10.14336/AD.2019.0228. eCollection 2019 Dec.

51. Castillo K, Nassif M, Valenzuela V, Rojas F, Matus S, Mercado G, et al. Trehalose delays the progression of amyotrophic lateral sclerosis by enhancing autophagy in motoneurons. *Autophagy.* 2013; **9**: 1308-20. doi: 10.4161/auto.25188. Epub 2013 Jun 6.

52. Zhang JJ, Zhou QM, Chen S, Le WD. Repurposing carbamazepine for the treatment of amyotrophic lateral sclerosis in SOD1-G93A mouse model. *CNS Neurosci Ther.* 2018; **24**: 1163-74. doi: 10.1111/cns.12855. Epub 2018 Apr 14.

53. Ueda T, Ito T, Kurita H, Inden M, Hozumi I. p-Coumaric Acid Has Protective Effects against Mutant Copper-Zinc Superoxide Dismutase 1 *via* the Activation of Autophagy in N2a Cells. *Int J Mol Sci* 2019; **20**: 2942. doi: 10.3390/ijms20122942.

54. Hetz C, Thielen P, Matus S, Nassif M, Court F, Kiffin R, et al. XBP-1 deficiency in the nervous system protects against amyotrophic lateral sclerosis by increasing autophagy. *Genes Dev*. 2009; **23**: 2294-

306. doi: 10.1101/gad.1830709. Epub 2009 Sep 17.

55. Imamura K, Izumi Y, Watanabe A, Tsukita K, Woltjen K, Yamamoto T, et al. The Src/c-Abl pathway is a potential therapeutic target in amyotrophic lateral sclerosis. *Sci Transl Med.* 2017; **9**: 3962. doi: 10.1126/scitranslmed.aaf3962.

56. Wong E, Cuervo AM. Autophagy gone awry in neurodegenerative diseases. *Nat Neurosci.* 2010; **13**: 805-11. doi: 10.1038/nn.2575.

57. Zhang X, Chen S, Song L, Tang Y, Shen Y, Jia L, et al. MTOR-independent, autophagic enhancer trehalose prolongs motor neuron survival and ameliorates the autophagic flux defect in a mouse model of amyotrophic lateral sclerosis. *Autophagy.* 2014; **10**: 588-602. doi: 10.4161/auto.27710. Epub 2014 Jan 15.

58. Switon K, Kotulska K, Janusz-Kaminska A, Zmorzynska J, Jaworski J. Molecular neurobiology of mTOR. *Neuroscience.* 2017; **341**: 112-53. doi: 10.1016/j.neuroscience.2016.11.017. Epub 2016 Nov 23.

59. Dutta K, Patel P, Julien JP. Protective effects of Withania somnifera extract in SOD1G93A mouse model of amyotrophic lateral sclerosis. *Exp Neurol.* 2018; **309**: 193-204. doi: 10.1016/j.expneurol.2018.08.008. Epub 2018 Aug 19.

Table

Due to technical limitations, Table 1 is provided in the Supplementary Files section.

Figures

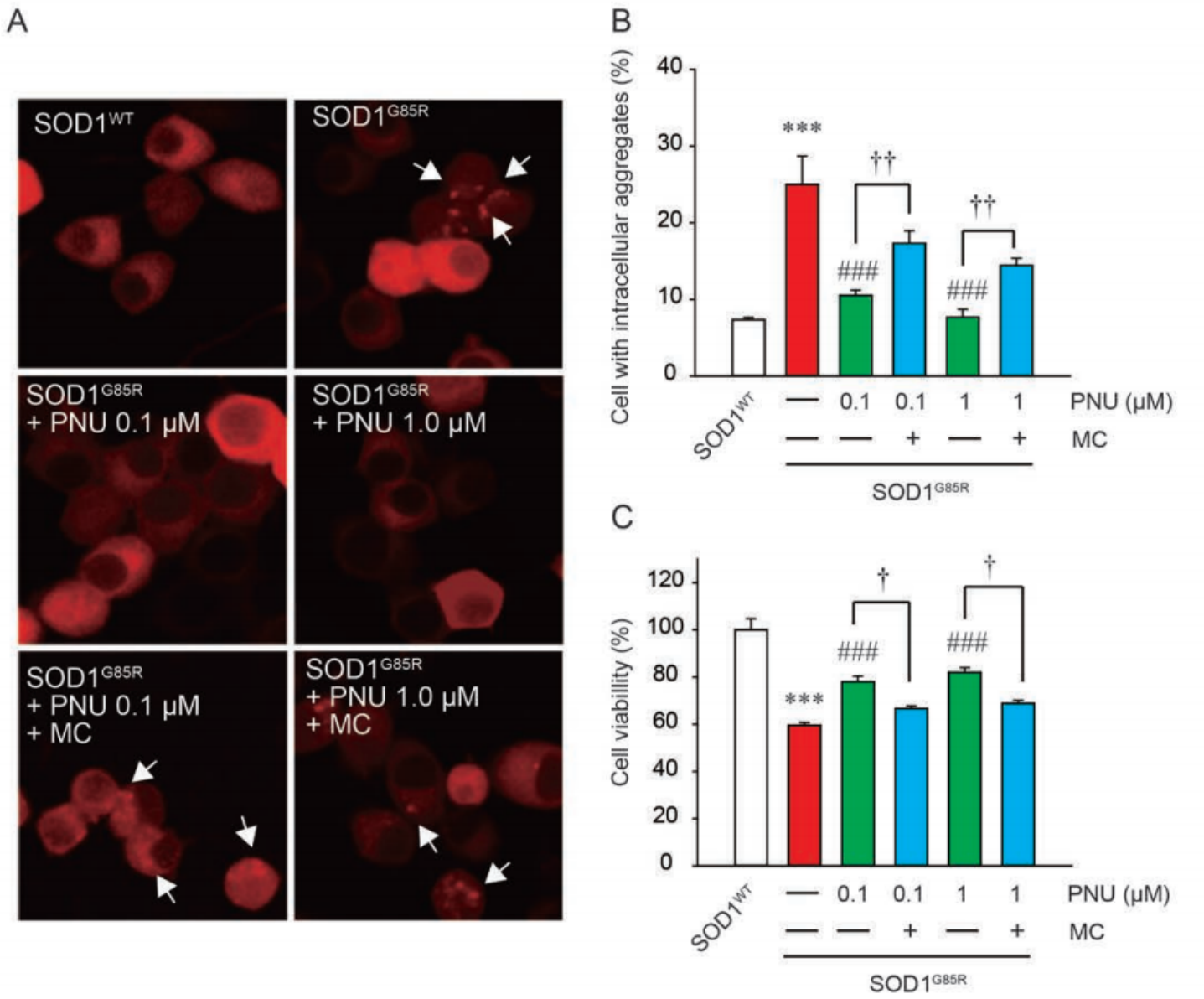

Figure 1

PNU282987 prevented SOD1G85R-induced neurotoxicity. N2a cells expressing mCherry-SOD1G85R were treated with 0.1 or 1 μM PNU282987 (PNU) in the presence or absence of 20 μM methyllycaconitine (MC). (A) Representative fluorescent microscopy images. Scale bar: 10 μm. (B) Quantified data of intracellular SOD1 aggregates. (C) The cell viability was measured by MTT assay. Data is expressed as mean ± SEM from three independent experiments. Significance: *** $p < 0.001$ vs. SOD1WT; ### $p < 0.001$ vs. SOD1G85R; † $p < 0.05$, †† $p < 0.01$ vs SOD1G85R with PNU282987.

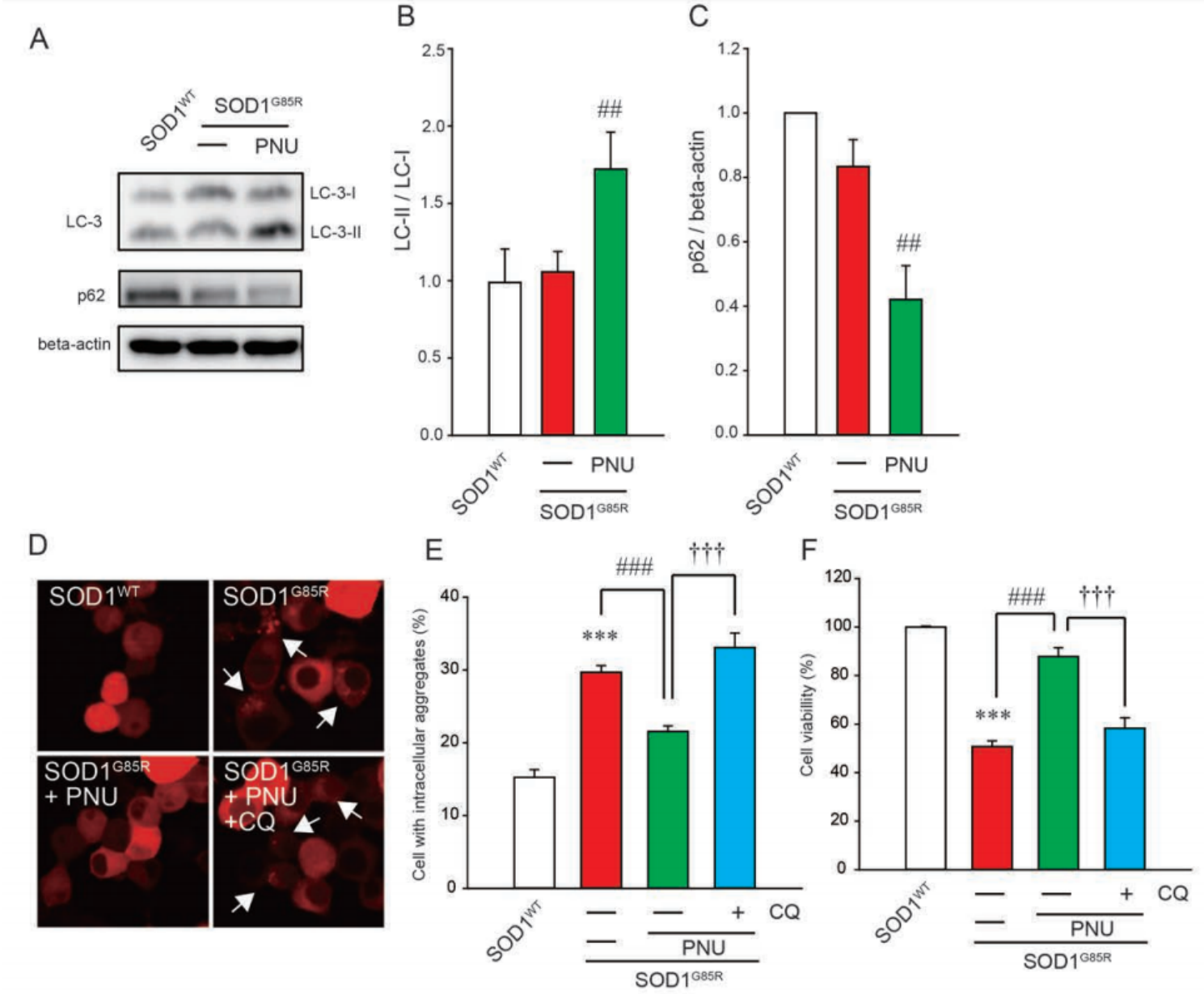

Figure 2

PNU282987 exerted the activation of autophagy. (A, B) N2a cells were transfected with SOD1G85R, and then incubated with 1 μM PNU282987. The lysates were analyzed by immunoblotting with anti-LC-3 (A) and p62 (B) and anti-β-actin antibodies. Levels normalized to the expression of β-actin and quantified based on the band density of SOD1WT. (C-D) N2a cells expressing mCherry-SOD1G85R were treated with 1 μM PNU282987 (PNU) in the presence or absence of 20 μM chloroquine (CQ). (C) Representative fluorescent microscopy images. Scale bar: 10 μm. (D) Quantified data of intracellular SOD1 aggregates. (E) The cell viability was measured by MTT assay. Data is expressed as mean ± SEM from three independent experiments. Significance: ### $p < 0.001$ vs. SOD1G85R.

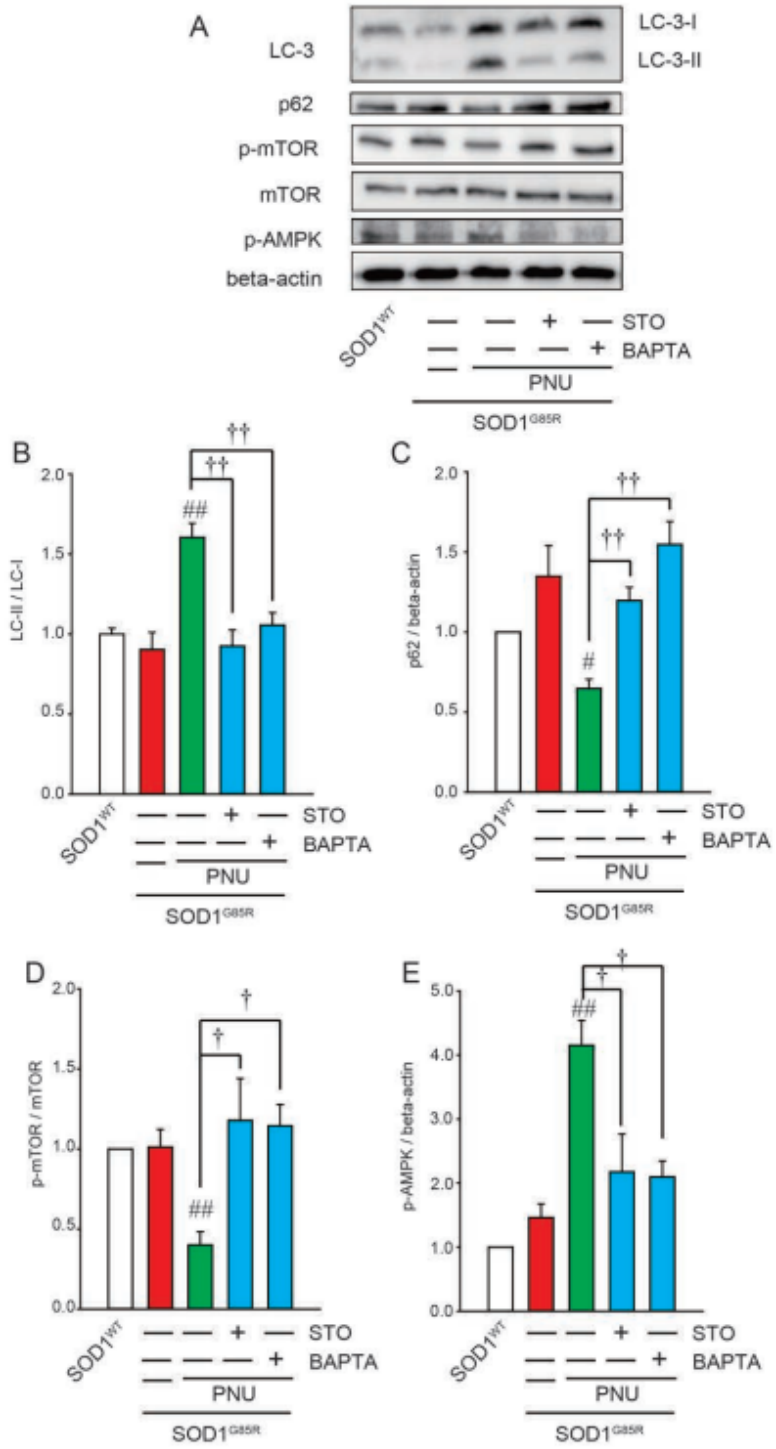

Figure 3

PNU282987-induced Ca2+ influx contributes to autophagy. Immunoblotting analysis of autophagy regulators with a Ca2+ chelator and CaMKK-specific inhibitor. N2a cells expressing SOD1G85R were treated with 1 μM PNU282987 (PNU) in the presence or absence of 1 μM STO609 (STO) or 1 μM BAPTA-AM (BAPTA). (A) The lysates were analyzed by immunoblotting with antibodies for LC-3, p62, phosphorylated mTOR (p-mTOR), mTOR, phosphorylated AMPK (p-AMPK), β-actin. (B-E) Relative levels

normalized by the expression of mTOR or β-actin were quantified, based on the density of SOD1WT. Data is expressed as mean ± SEM from three independent experiments. Significance: # $p < 0.05$, ## $p < 0.01$ vs. SOD1G85R; † $p < 0.05$, †† $p < 0.01$ vs SOD1G85R with PNU282987.

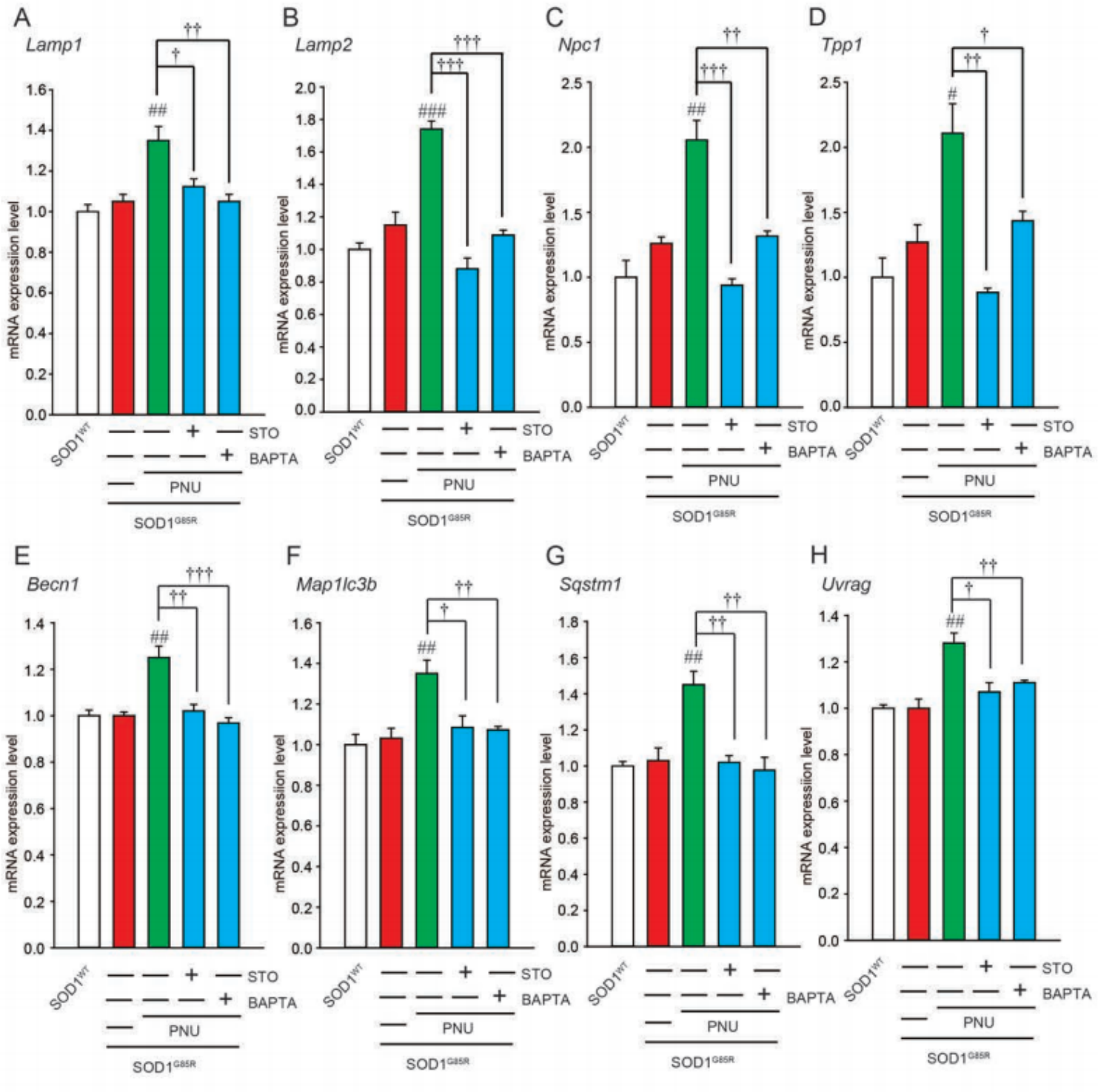

Figure 4

Effects of PNU282987 on transcription factor EB (TFEB) related mRNA expression. (A-H) N2a cells expressing mCherry-SOD1G85R were treated with 1 μM PNU282987 (PNU) in the presence or absence of 1 μM STO609 (STO) and 1 μM BAPTA-AM (BAPTA). At 24 h after treatment with PNU, mRNA expressions

of Lamp1 (A), Lamp2 (B), Npc1 (C), Tpp1 (D), Becn1 (E), Map1lc3b (F), Sqstm1 (G), Uvrag (H) were analyzed using the SYBR Green-based RT-qPCR assay. The expression levels of mRNA were normalized to the expression levels of β-actin mRNA. Significance: # $p < 0.05$, ## $p < 0.01$, ### $p < 0.01$ vs. SOD1G85R; † $p < 0.05$, †† $p < 0.01$, ††† $p < 0.01$ vs SOD1G85R with PNU282987.

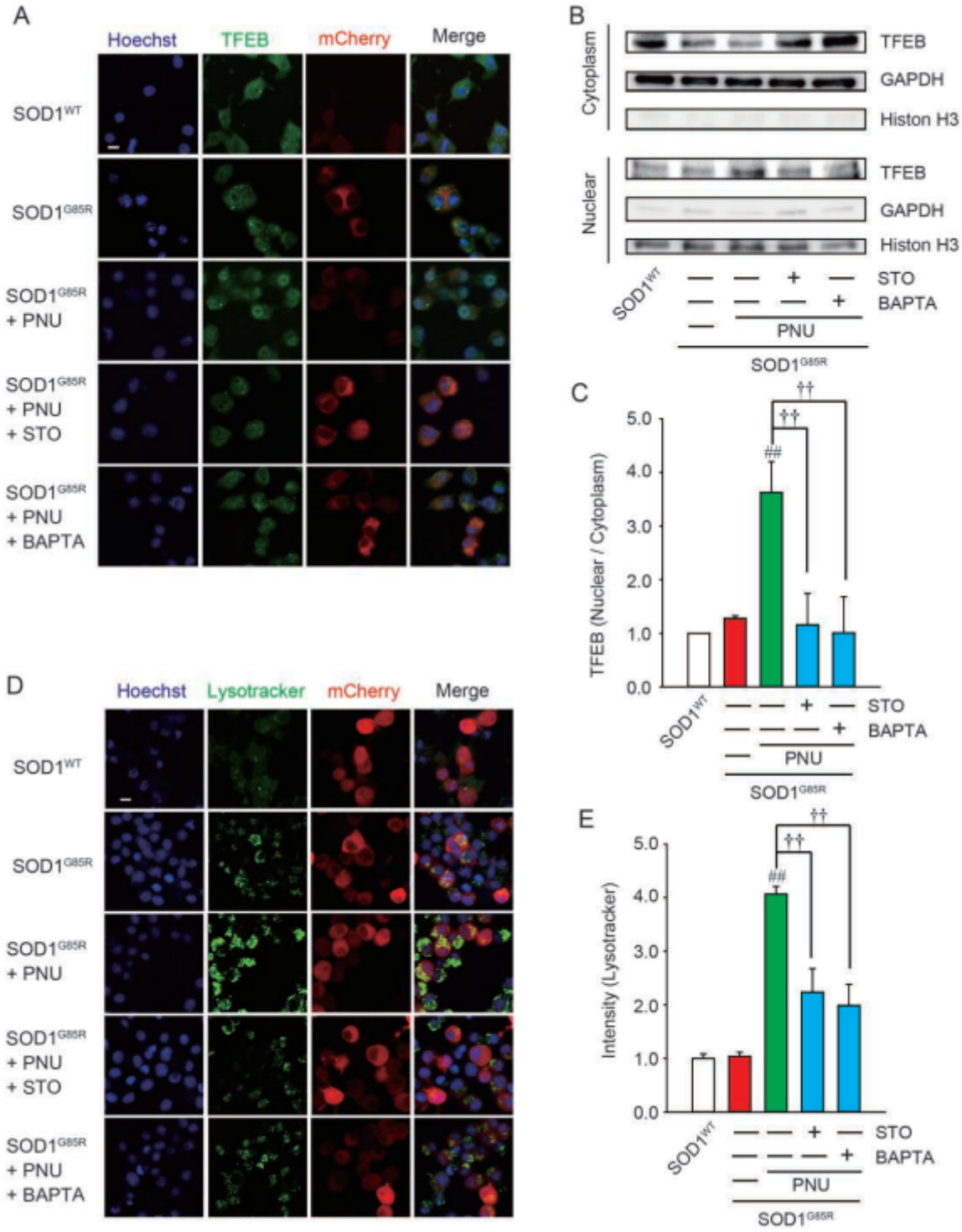

Figure 5

PNU282987 enhances TFEB activity. N2a cells expressing SOD1G85R were treated with 1 μM PNU282987 (PNU) in the presence or absence of 1 μM STO609 (STO) or 1 μM BAPTA-AM (BAPTA). (A) Representative fluorescent microscopy images of TFEB. Scale bar: 10 μm. (B) After the fractionation using NE-PER™ Nuclear and Cytoplasmic Extraction Reagents, the lysates were analyzed by immunoblotting with antibodies for TFEB, GAPDH, and Histone H3. (C) The ratio of nuclear to cytosolic TFEB was calculated and analyzed. (D) Representative fluorescent microscopy images of lysotracker. Scale bar: 10 μm. (E) Quantified data of lysotracker intensity. Significance: ## $p < 0.01$ vs. SOD1G85R; †† $p < 0.01$ vs. SOD1G85R with PNU282987.

Supplementary Files

This is a list of supplementary files associated with this preprint. Click to download.

- 200624NicotineSOD1Table.xls
- 200624NicotineSOD1Table.xls
- 200624NicotineSOD1Table.xls